Geophys. J. Int. (1998) **134**, 677–688

Multiple scattering of *SH* waves by imperfectly bonded interfaces with inhomogeneous strengths

Yoshio Murai* and Teruo Yamashita

Earthquake Research Institute, University of Tokyo, 1-1-1 Yayoi, Bunkyo-ku, Tokyo 113-0032, Japan

Accepted 1998 March 4. Received 1998 March 4; in original form 1996 December 5

SUMMARY

We have developed a new, simple method to calculate elastic waves scattered by zonally distributed cracks, taking account of multiple crack interactions. In this paper, our method is applied to *SH*-wave propagation in 2-D elastic media. An array of cracks is represented by an imperfectly bonded interface with a spatially inhomogeneous strength. A section of the interface with vanishing strength represents a stress-free crack, while a section with a significantly high elastic stiffness approximates an intact section. A cracked zone is therefore represented by a multilayered zone, partitioned by many such interfaces. In this formation, the interactions among all cracks can be considered implicitly and a mixed boundary-value problem can be circumvented.

In our method, the elastic waves scattered by an interface are expanded into discrete reflected and transmitted plane-wave components. The wavefield in a cracked zone can be easily calculated by the wave propagator method or by the reflection and transmission operator method, on the basis of this expansion. The accuracy of our method is shown to be quite satisfactory for some examples.

The zeroth-order reflection coefficient, which is defined as the coefficient for a reflected-wave component that has a reflection angle equal to the incidence angle, is specifically studied for some crack arrays, as an example of the application of our method of analysis.

Key words: cracks, layered media, numerical techniques, *S* waves, scattering, wave propagation.

1 INTRODUCTION

It is known that the Earth's crust is permeated by large numbers of cracks. In particular, fault zones are highly fractured and the presence of densely distributed cracks is revealed by televiewer observations in boreholes (e.g. Malin *et al.* 1988). It has also been confirmed, by observations of shear-wave splitting and polarization anomalies of *P*-wave first motions, that there exists a dense distribution of cracks aligned parallel to the fault plane within a fault zone (e.g. Leary, Li & Aki 1987; Li, Leary & Aki 1987). Cracks generally cause scattering of incident elastic waves. The crack interactions cannot be neglected in treating problems of scattering in a medium with densely distributed cracks, such as in a fault zone. Some authors have given theoretical treatments of elastic-wave scattering due to distributed cracks on the basis of the mean-wave formalism and the approximation introduced by Foldy (1945) (e.g. Kikuchi 1981a,b; Yamashita 1990; Kawahara & Yamashita 1992). This approximation neglects crack interactions, so it is valid when the density of cracks is low. On the other hand, Murai, Kawahara & Yamashita (1995) rigorously treated multiple crack interactions by applying a boundary integral equation method (BIEM) to the crack scattering problem. They could not, however, deal with large numbers of cracks, because they faced the difficulty of memory and CPU-time limits, which is common in many traditional methods.

In this paper, we propose a method to treat multiple crack interactions more efficiently. The deformation is assumed to be of *SH* type for simplicity. In our method of analysis, an array of cracks is represented by an imperfectly bonded interface with a spatially inhomogeneous strength. A section of the interface with vanishing strength represents a stress-free crack, while a section with a significantly high elastic stiffness approximates an intact section. A cracked zone is therefore represented by a multilayered zone, partitioned by many such interfaces. It is easy to introduce an arbitrary coupling of crack surfaces by means of this approach because each interface can

* Now at: Institute of Seismology and Volcanology, Graduate School of Science, Hokkaido University, N-10 W-8, Kita-ku, Sapporo 060-0810, Japan. E-mail: murai@lobs.sci.hokudai.ac.jp.

be assumed to be bonded with an arbitrarily inhomogeneous strength.

In our method, elastic waves scattered by an interface are expanded into discrete reflected and transmitted plane-wave components. The wavefield in the multilayered zone can be calculated by the wave propagator method (Kennett 1983) or by the reflection and transmission operator method (Kennett 1984). Multiple crack interactions can be treated implicitly in this method of analysis, which greatly simplifies the analysis of elastic-wave scattering due to densely distributed cracks. In addition, it is advantageous that the introduction of a low-velocity zone is quite easy, because we have only to consider the reflection and transmission of plane waves (Murai 1994). It is shown below that the accuracy of our method is satisfactory for some simple examples whose analytical or numerical solutions are known.

In general, we introduce a viscoelastic constitutive friction law at each crack on the basis of the following field and laboratory observations. Water-saturated cracks are directly observable in the shallow crust (e.g. Malin *et al.* 1988), and their existence in the deeper part of the crust is likely, from a geological point of view (e.g. Takeshita & Karato 1989). It is quite reasonable to assume that water-saturated cracks cause viscoelastic friction at their surfaces. In addition, it has been shown in laboratory experiments with rock samples that fracture surfaces behave viscoelastically in the transmission of elastic waves even under dry conditions (Yoshioka & Kikuchi 1993).

2 EXPANSION OF WAVES SCATTERED BY A SINGLE INTERFACE INTO DISCRETE PLANE-WAVE COMPONENTS

In this section, we propose a method to calculate the response of an imperfectly bonded interface with a spatially inhomogeneous strength to an incident plane wave, which is fundamental to the subsequent analyses. We assume an elastic medium consisting of two half-spaces separated by an interface, and define the coordinate system (x, y) so that the x-axis coincides with the interface (Fig. 1). Each half-space is assumed to have the same elastic properties. The mechanical coupling at the interface is assumed to be characterized by a specific stiffness function $k_T(x)$ and a specific viscosity function $\eta^*(x)$. The specific stiffness is defined as the ratio of an increment in stress to the corresponding increase in relative displacement.

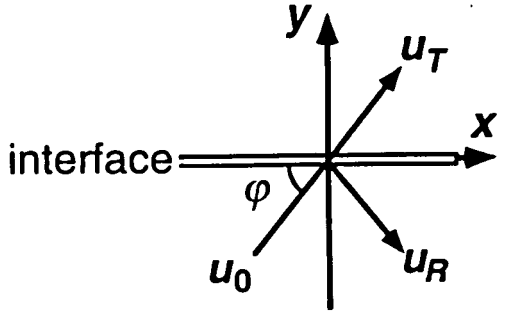

Figure 1. Reflection and transmission at an imperfectly bonded interface. The x-axis coincides with the interface, and φ is the angle between the x-axis and the propagation direction of the incident plane wave.

The specific viscosity denotes the viscous resistance per unit length of the interface to the relative displacement. Such a coupling has been assumed on a crack face by many researchers (e.g. Schoenberg & Douma 1988; Nagy 1992; Pyrak-Nolte & Cook 1987; Hudson, Liu & Crampin 1996). What forms a striking contrast between our study and the previous ones is that an array of arbitrarily distributed cracks is represented by a spatially inhomogeneous distribution of the specific stiffness in our study: a section with $k_T(x) = 0$ and $\eta^*(x) = 0$ denotes a stress-free crack, while a section with a significantly large $k_T(x)$ approximates an intact section. Our approach has an advantage because it can circumvent a mixed boundary-value problem that has to be solved in the traditional approach to the crack scattering problem.

The specific stiffness controls a slip-strengthening behaviour of the fracture surface. It has been shown by laboratory experiments on stick–slip friction that a slip-strengthening process precedes an unstable slip failure due to dynamic rupture propagation (Ohnaka, Kuwahara & Yamamoto 1987). The relative displacement of the interface caused by an incident elastic wave is assumed to be comparatively small and the incident wave does not cause a dynamic rupture propagation in this study.

An incident plane *SH* wave is assumed in the form

$$u_0(x, y) = \exp[ik(x \cos\varphi + y \sin\varphi)], \tag{1}$$

where i is the square root of -1, k is the wavenumber and φ is the angle between the x-axis and the propagation direction of the incident plane wave. Here the time factor $\exp(-i\omega t)$ is omitted for brevity, where $\omega = k\beta$ and β is the shear-wave velocity of the matrix. The scattered waves are represented as a superposition of plane waves in the form

$$u_R(x, y) = \frac{i}{2\pi}\int_{-\infty}^{\infty} A_1(s)\exp[isx + \beta_2(s)y]ds \quad \text{for } y < 0, \tag{2}$$

$$u_T(x, y) = \frac{i}{2\pi}\int_{-\infty}^{\infty} A_2(s)\exp[isx - \beta_2(s)y]ds \quad \text{for } y > 0, \tag{3}$$

where $u_R(x, y)$ and $u_T(x, y)$ are the reflected and transmitted waves, respectively; $A_1(s)$ and $A_2(s)$ are unknown functions; and $\beta_2(s) = (s^2 - k^2)^{1/2} = -i(k^2 - s^2)^{1/2}$. The boundary conditions on the interface are

$$\mu\frac{\partial}{\partial y}u_T(x, y) = \mu\frac{\partial}{\partial y}[u_0(x, y) + u_R(x, y)] \tag{4}$$

$$= [k_T(x) - i\beta k\eta^*(x)]\phi(x) \quad \text{for } y = 0, \tag{5}$$

where $\phi(x)$ is the relative displacement at the interface and μ is the rigidity. Eq. (4) is the condition that the stress is continuous across the interface and eq. (5) represents the condition of coupling at the interface.

From eqs (1)–(3) we can rewrite the condition (4) as

$$\frac{1}{2\pi}\int_{-\infty}^{\infty}\beta_2(s)[A_1(s) + A_2(s)]\,e^{isx}ds = -k\exp(ikx\cos\varphi)\sin\varphi. \tag{6}$$

An inverse Fourier transformation gives

$$A_1(s) + A_2(s) = -2\pi k\sin\varphi\frac{\delta(s - k\cos\varphi)}{\beta_2(s)}, \tag{7}$$

where δ is the Dirac delta function. Upon using eq. (7), eq. (5) yields

$$\frac{\mathrm{i}}{\pi}[k_T(x)-\mathrm{i}\beta k\eta^*(x)]\int_{-\infty}^{\infty}A_2(s)\,\mathrm{e}^{\mathrm{i}sx}ds+\frac{\mathrm{i}\mu}{2\pi}\int_{-\infty}^{\infty}\beta_2(s)A_2(s)\,\mathrm{e}^{\mathrm{i}sx}ds$$
$$=2[k_T(x)-\mathrm{i}\beta k\eta^*(x)]\exp(\mathrm{i}kx\cos\varphi). \quad (8)$$

This integral equation for $A_2(s)$ cannot be solved analytically for arbitrary functions $k_T(x)$ and $\eta^*(x)$.

We expand the function $k_T(x)-\mathrm{i}\beta k\eta^*(x)$ as a Fourier series as follows:

$$k_T(x)-\mathrm{i}\beta k\eta^*(x)=\sum_{j=-N}^{N}K_j\exp(2\pi\mathrm{i}j\Delta sx), \quad (9)$$

where N is a large positive number. By substituting eq. (9) into eq. (8) and carrying out a Fourier transformation with respect to x, we obtain

$$2\mathrm{i}\sum_{j=-N}^{N}K_jA_2(s-2\pi j\Delta s)+\mathrm{i}\mu\beta_2(s)A_2(s)$$
$$=4\pi\sum_{j=-N}^{N}K_j\delta(s-k\cos\varphi-2\pi j\Delta s). \quad (10)$$

The solution of eq. (10) can be written as

$$A_2(s)=\sum_{m=-\infty}^{\infty}C_m(s)\delta(s-k\cos\varphi-2\pi m\Delta s). \quad (11)$$

After using eqs (7) and (11), eqs (2) and (3) are reduced to

$$u_R(x,y)=\exp[\mathrm{i}k(x\cos\varphi-y\sin\varphi)]$$
$$-\frac{\mathrm{i}}{2\pi}\sum_{m=-\infty}^{\infty}C_m(k\cos\varphi+2\pi m\Delta s)$$
$$\times\exp[\mathrm{i}(k\cos\varphi+2\pi m\Delta s)x$$
$$+\beta_2(k\cos\varphi+2\pi m\Delta s)y] \quad \text{for } y<0, \quad (12)$$

$$u_T(x,y)=\frac{\mathrm{i}}{2\pi}\sum_{m=-\infty}^{\infty}C_m(k\cos\varphi+2\pi m\Delta s)$$
$$\times\exp[\mathrm{i}(k\cos\varphi+2\pi m\Delta s)x$$
$$-\beta_2(k\cos\varphi+2\pi m\Delta s)y] \quad \text{for } y>0. \quad (13)$$

Thus the reflected and transmitted waves are expanded into discrete plane-wave components. Here, $C_m(k\cos\varphi+2\pi m\Delta s)$ is unknown and we rewrite it as

$$C_m=C_m(k\cos\varphi+2\pi m\Delta s) \quad (14)$$

for brevity.

If the series (11), (12) and (13) converge, they can be truncated at $|m|=n(\gg 1)$. After the truncated form of eq. (11) is substituted into eq. (10), we have

$$2\mathrm{i}\sum_{j=-N}^{N}\sum_{m=-n}^{n}K_jC_m\delta[s-k\cos\varphi-2\pi(j+m)\Delta s]$$
$$+\mathrm{i}\mu\beta_2(s)\sum_{m=-n}^{n}C_m\delta(s-k\cos\varphi-2\pi m\Delta s)$$
$$=4\pi\sum_{j=-N}^{N}K_j\delta(s-k\cos\varphi-2\pi j\Delta s). \quad (15)$$

If $s=k\cos\varphi+2\pi l\Delta s$ ($l=0,\pm1,\pm2,\ldots,\pm n$) is assumed, we can obtain the following simultaneous equations for C_m from eq. (15):

$$\sum_{\substack{j=-N\\ j\neq 0}}^{N}Q_jC_{l-j}+P_lC_l=S_l \quad \text{for } l=0,\pm1,\pm2,\ldots,\pm N, \quad (16)$$

$$\sum_{\substack{j=-N\\ j\neq 0}}^{N}Q_jC_{l-j}+P_lC_l=0$$
$$\text{for } l=\pm(N+1),\pm(N+2),\ldots,\pm n, \quad (17)$$

where

$$\left.\begin{aligned}P_l&=2\mathrm{i}K_0+\mathrm{i}\mu\beta_2(k\cos\varphi+2\pi l\Delta s)\\ &\qquad \text{for } l=0,\pm1,\pm2,\ldots,\pm n,\\ Q_j&=2\mathrm{i}K_j \quad \text{for } j=\pm1,\pm2,\ldots,\pm N,\\ S_l&=4\pi K_l \quad \text{for } j=0,\pm1,\pm2,\ldots,\pm N.\end{aligned}\right\} \quad (18)$$

Once eqs (16) and (17) are solved, the reflected and transmitted waves can be determined from the truncated forms of eqs (12) and (13) with eq. (14).

3 WAVEFIELD IN A MULTILAYERED ZONE

In this section, we formulate a method to calculate the wavefield in a multilayered zone partitioned by N_s parallel interfaces imperfectly bonded with inhomogeneous strengths (Fig. 2). Each layer is assumed to have the same elastic properties. This zone is a model of a fault zone consisting of distributed, parallel cracks. We can expand the scattered waves into discrete plane-wave components and obtain the plane-wave reflection and transmission coefficients at each interface, as stated in the preceding section. Hence the displacement field in each layer can be represented as the superposition of discrete plane-wave components, and it can be calculated by the wave propagator method (Kennett 1983) or by the reflection and transmission operator method (Kennett 1984).

Now we define the local coordinate system (x_j, y_j) fixed at the jth interface ($j=1,\ldots,N_s$) and the global coordinate

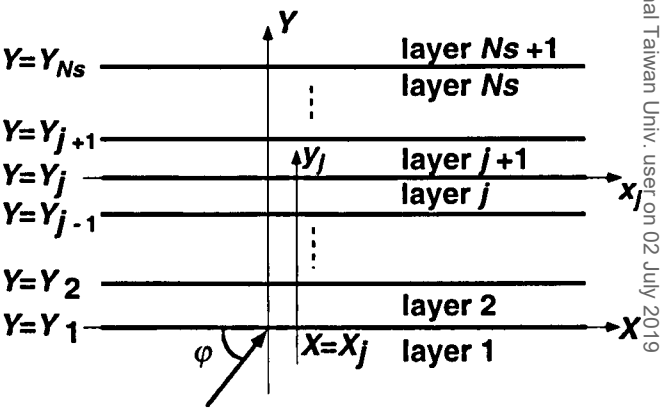

Figure 2. A multilayered medium partitioned by N_s parallel imperfectly bonded interfaces with inhomogeneous strengths. A local coordinate system is defined at each interface: the system (x_j, y_j) is fixed at the jth interface ($j=1,\ldots,N_s$). The global coordinate system (X, Y) is the same as the local coordinate system (x_1, y_1). The origin of the local coordinate system (x_j, y_j) is denoted by (X_j, Y_j) in the global coordinate system; φ is the angle between the X-axis and the propagation direction of the incident plane wave.

system (X, Y) (Fig. 2). The x_j-axis coincides with the jth interface and the origin of the local coordinate system is located at an arbitrary point on the interface. The global coordinate system (X, Y) coincides with the local coordinate system (x_1, y_1). The origin of the local coordinate system (x_j, y_j) is denoted by (X_j, Y_j) in the global coordinate system. We assume a harmonic, plane, incident *SH* wave of the form

$$u_0(X, Y) = \exp[ik(X \cos\varphi + Y \sin\varphi)]. \tag{19}$$

3.1 Formulation using the wave propagator method

We divide the displacement field in each layer into a homogeneous and an inhomogeneous (or evanescent) wave. The displacement field in the jth layer is represented as

$$u_j^+ = u_j^{(h)+} + u_j^{(e)+}, \tag{20}$$

$$u_j^- = u_j^{(h)-} + u_j^{(e)-}, \tag{21}$$

where '(h)' and '(e)' denote the homogeneous and evanescent wave components, respectively, and the symbols '+' and '−' denote the wave components propagating in the positive and negative directions of the Y-axis, respectively. Hereafter we refer to the waves propagating in the positive and negative directions of the Y-axis as the upgoing and downgoing waves, respectively.

First, we consider the homogeneous waves. The displacement field in each layer is written as the superposition of discrete plane-wave components in the forms

$$u_1^{(h)+}(x_1, y_1) = e_0^{(-1)}, \tag{22}$$

$$u_1^{(h)-}(x_1, y_1) = \sum_{m=-n_q}^{n_p} B_{1m} e_m^{(+1)}, \tag{23}$$

$$u_j^{(h)+}(x_j, y_j) = \sum_{m=-n_q}^{n_p} A_{jm} e_m^{(-j)} \quad \text{for } j = 1, \ldots, N_s, \tag{24}$$

$$u_j^{(h)-}(x_{j-1}, y_{j-1}) = \sum_{m=-n_q}^{n_p} B_{jm} e_m^{[+(j-1)]} \quad \text{for } j = 1, \ldots, N_s, \tag{25}$$

$$u_{N_s+1}^{(h)+}(x_{N_s}, y_{N_s}) = \sum_{m=-n_q}^{n_p} A_{N_s+1,m} e_m^{(-N_s)}, \tag{26}$$

where

$$e_m^{(\pm j)} = \exp[i(k \cos\varphi + 2\pi m \Delta s)x_j \pm \beta_2(k \cos\varphi + 2\pi m \Delta s)y_j]. \tag{27}$$

The wave component $e_m^{(\pm j)}$ is assumed to represent a homogeneous plane wave in the range $-n_q \le m \le n_p$; it behaves as an evanescent wave outside this range. The coefficients A_{jm} and B_{jm} of the plane-wave components in each layer are obtained from the reflection and transmission coefficients at each interface, as shown below. (See Appendix A for the notation used for the reflection and transmission coefficients.)

We define the vectors comprising the coefficients of the plane-wave components as

$$\mathbf{A}_j = (A_{j,-n_q} \ldots A_{j0} \ldots A_{jn_p})^T \quad \text{for } j = 2, \ldots, N_s + 1, \tag{28}$$

$$\mathbf{B}_j = (B_{j,-n_q} \ldots B_{j0} \ldots B_{jn_p})^T \quad \text{for } j = 1, \ldots, N_s, \tag{29}$$

$$\mathbf{A}_1 = (0 \ldots 0\,1\,0 \ldots 0)^T. \tag{30}$$

We define the reflection matrix $\mathbf{R}_j$ and the transmission matrix $\mathbf{T}_j$ of the jth interface for upward incidence by

$$\mathbf{R}_j = (R_{ml}^{(+j)}) \quad \text{for } j = 1, \ldots, N_s,$$

$$\mathbf{T}_j = (T_{ml}^{(+j)}) \quad \text{for } j = 1, \ldots, N_s \tag{31}$$

$(m = -n_q, \ldots, n_p;\ l = -n_q, \ldots, n_p)$, and $\mathbf{R}_{-j}$ and $\mathbf{T}_{-j}$ for downward incidence by

$$\mathbf{R}_{-j} = (R_{ml}^{(-j)}) \quad \text{for } j = 1, \ldots, N_s - 1,$$

$$\mathbf{T}_{-j} = (T_{ml}^{(-j)}) \quad \text{for } j = 1, \ldots, N_s - 1 \tag{32}$$

$(m = -n_q, \ldots, n_p;\ l = -n_q, \ldots, n_p)$. The elements of these matrices are reflection and transmission coefficients. Upon considering reflection and transmission at the jth interface $(j = 1, \ldots, N_s - 1)$, we obtain the following form of the wave propagator:

$$\begin{pmatrix} \mathbf{A}_{j+1} \\ \mathbf{B}_{j+1} \end{pmatrix} = \begin{pmatrix} \mathbf{T}_j - \mathbf{R}_{-j}\mathbf{T}_{-j}^{-1}\mathbf{R}_j & \mathbf{R}_{-j}\mathbf{T}_{-j}^{-1} \\ -\mathbf{T}_{-j}^{-1}\mathbf{R}_j & \mathbf{T}_{-j}^{-1} \end{pmatrix} \begin{pmatrix} \mathbf{A}_j \\ \mathbf{B}_j \end{pmatrix}. \tag{33}$$

For the N_sth interface, we get

$$\begin{pmatrix} \mathbf{A}_{N_s+1} \\ \mathbf{0} \end{pmatrix} = \begin{pmatrix} \mathbf{T}_{N_s} & \mathbf{0} \\ -\mathbf{R}_{N_s} & \mathbf{I} \end{pmatrix} \begin{pmatrix} \mathbf{A}_{N_s} \\ \mathbf{B}_{N_s} \end{pmatrix}, \tag{34}$$

where $\mathbf{I}$ is the identity operator, since no interface exists above the N_sth one and no downgoing waves are incident on the N_sth interface. The displacement field in each layer can be calculated by using eqs (30), (33) and (34).

Next, we consider the evanescent waves. The evanescent waves are treated separately in this paper since $\mathbf{T}_j^{-1}$ diverges numerically if the evanescent waves are included in the calculation of the wave propagator in eq. (33): note that we have the relations $T_{ml}^{(+j)} \approx 0$ and $T_{ml}^{(-j)} \approx 0$ for $m \le -n_q - 1$ or $m \ge n_p + 1$ in eqs (31) and (32) because of the concentration of the energy of the evanescent wave near an interface.

The displacement field near the jth interface $(j = 1, \ldots, N_s)$ is written as follows:

$$u_{j+1}^{(e)+}(x_j, y_j) = \sum_{m=-n_e}^{-n_q-1} A_{j+1,m} e_m^{(-j)} + \sum_{m=n_p+1}^{n_e} A_{j+1,m} e_m^{(-j)}, \tag{35}$$

$$u_j^{(e)-}(x_j, y_j) = \sum_{m=-n_e}^{-n_q-1} B_{jm} e_m^{(+j)} + \sum_{m=n_p+1}^{n_e} B_{jm} e_m^{(+j)}, \tag{36}$$

where n_e determines the number of discrete plane-wave components. The coefficients $A_{j+1,m}$ and B_{jm} are obtained from the reflection and transmission coefficients for the evanescent waves at the jth interface. Now we use the same notation for the reflection and transmission coefficients for the evanescent waves as for the homogeneous waves (see Appendix A). When an upgoing wave component $e_l^{(-j)}$ is assumed to be incident on the jth interface, the reflected evanescent waves are expanded into the downgoing evanescent plane-wave components $R_{ml}^{(+j)} e_m^{(+j)} (m = -n_e, \ldots, -n_q - 1, n_p + 1, \ldots, n_e)$ and the transmitted evanescent waves are expanded into the upgoing evanescent plane-wave components $T_{ml}^{(+j)} e_m^{(-j)}$ $(m = -n_e, \ldots, -n_q - 1, n_p + 1, \ldots, n_e)$, where $R_{ml}^{(+j)}$ and $T_{ml}^{(+j)}$ are the reflection and transmission coefficients for the evanescent waves at the jth interface. The reflection and transmission coefficients for an incident downgoing wave component are denoted by $R_{ml}^{(-j)}$ and $T_{ml}^{(-j)}$ in the same way. Eqs (12) and (13) suggest that the reflection and transmission coefficients

for the evanescent waves are written in the forms

$$R_{ml}^{(+j)} = R_{ml}^{(-j)} = -\frac{\mathrm{i}}{2\pi} C_{ml}^{(j)}, \tag{37}$$

$$T_{ml}^{(+j)} = T_{ml}^{(-j)} = \frac{\mathrm{i}}{2\pi} C_{ml}^{(j)}; \tag{38}$$

see Appendix A for the definition of $C_{ml}^{(j)}$.

We define the vectors comprising the coefficients of the plane-wave components of the evanescent waves as

$$\mathbf{A}_j^{(\mathrm{e})} = (A_{j-n_\mathrm{e}} \dots A_{j-n_\mathrm{q}-1} A_{jn_\mathrm{p}+1} \dots A_{jn_\mathrm{e}})^\mathrm{T} \quad \text{for } j = 2, \dots, N_\mathrm{s}+1, \tag{39}$$

$$\mathbf{B}_j^{(\mathrm{e})} = (\mathbf{B}_{j-n_\mathrm{e}} \dots \mathbf{B}_{j-n_\mathrm{q}-1} \mathbf{B}_{jn_\mathrm{p}+1} \dots \mathbf{B}_{jn_\mathrm{e}})^\mathrm{T} \quad \text{for } j = 1, \dots, N_\mathrm{s}, \tag{40}$$

and the reflection and transmission matrices, whose entries are reflection and transmission coefficients for evanescent waves, as

$$\mathbf{R}_j^{(\mathrm{e})} = (R_{ml}^{(+j)}) \quad \text{for } j = 1, \dots, N_\mathrm{s},$$

$$\mathbf{T}_j^{(\mathrm{e})} = (T_{ml}^{(+j)}) \quad \text{for } j = 1, \dots, N_\mathrm{s} \tag{41}$$

($m = -n_\mathrm{e}, \dots, -n_\mathrm{q}-1, n_\mathrm{p}+1, \dots, n_\mathrm{e}$; $l = -n_\mathrm{q}, \dots, n_\mathrm{p}$). Upon considering reflection and transmission of the jth interface ($j = 1, \dots, N_\mathrm{s}-1$), we obtain the following relations for the evanescent waves:

$$\begin{pmatrix} \mathbf{A}_{j+1}^{(\mathrm{e})} \\ \mathbf{B}_j^{(\mathrm{e})} \end{pmatrix} = \begin{pmatrix} \mathbf{T}_j^{(\mathrm{e})} & \mathbf{R}_j^{(\mathrm{e})} \\ \mathbf{R}_j^{(\mathrm{e})} & \mathbf{T}_j^{(\mathrm{e})} \end{pmatrix} \begin{pmatrix} \mathbf{A}_j \\ \mathbf{B}_{j+1} \end{pmatrix}. \tag{42}$$

For the N_sth interface, we obtain

$$\begin{pmatrix} \mathbf{A}_{N_\mathrm{s}+1}^{(\mathrm{e})} \\ \mathbf{B}_{N_\mathrm{s}}^{(\mathrm{e})} \end{pmatrix} = \begin{pmatrix} \mathbf{T}_{N_\mathrm{s}}^{(\mathrm{e})} \\ \mathbf{R}_{N_\mathrm{s}}^{(\mathrm{e})} \end{pmatrix} \mathbf{A}_{N_\mathrm{s}}. \tag{43}$$

Because $\mathbf{A}_j$ and $\mathbf{B}_j$ are obtained from eqs (30), (33) and (34), $\mathbf{A}_j^{(\mathrm{e})}$ and $\mathbf{B}_j^{(\mathrm{e})}$ can be calculated from eqs (42) and (43).

Thus we can calculate the displacement field anywhere in the medium by means of eqs (20)–(26), (35) and (36).

3.2 Formulation using the reflection and transmission operator method

The displacement field in each layer is written as a superposition of discrete plane-wave components in the forms

$$u_1^+(x_1, y_1) = e_0^{(-1)}, \tag{44}$$

$$u_1^-(x_1, y_1) = \sum_{m=-n_\mathrm{r}}^{n_\mathrm{r}} B_{1m} e_m^{(+1)}, \tag{45}$$

$$u_j^+(x_j, y_j) = \sum_{m=-n_\mathrm{r}}^{n_\mathrm{r}} A_{jm} e_m^{(-j)} \quad \text{for } j = 1, \dots, N_\mathrm{s}, \tag{46}$$

$$u_j^-(x_{j-1}, y_{j-1}) = \sum_{m=-n_\mathrm{r}}^{n_\mathrm{r}} B_{jm} e_m^{[+(j-1)]} \quad \text{for } j = 1, \dots, N_\mathrm{s}, \tag{47}$$

$$u_{N_\mathrm{s}+1}^+(x_{N_\mathrm{s}}, y_{N_\mathrm{s}}) = \sum_{m=-n_\mathrm{r}}^{n_\mathrm{r}} A_{N_\mathrm{s}+1\,m} e_m^{(-N_\mathrm{s})}, \tag{48}$$

where $e_m^{(\pm j)}$ is defined by eq. (27) and n_r determines the number of discrete plane-wave components. Note that both the homogeneous and the evanescent waves are included in eqs (45)–(48). The coefficients A_{jm} and B_{jm} of the plane-wave components in each layer are obtained from the reflection and transmission coefficients at each interface. The reflection and transmission coefficients at each interface are derived in Appendix A. We define the vectors comprising the coefficients of the plane-wave components as

$$\mathbf{A}_j = (A_{j-n_\mathrm{r}} \dots A_{j0} \dots A_{jn_\mathrm{r}})^\mathrm{T} \quad \text{for } j = 2, \dots, N_\mathrm{s}+1, \tag{49}$$

$$\mathbf{B}_j = (B_{j-n_\mathrm{r}} \dots B_{j0} \dots B_{jn_\mathrm{r}})^\mathrm{T} \quad \text{for } j = 1, \dots, N_\mathrm{s}, \tag{50}$$

$$\mathbf{A}_1 = (0 \dots 010 \dots 0)^\mathrm{T}, \tag{51}$$

and the reflection and transmission matrices of the jth interface, whose entries are reflection and transmission coefficients, as

$$\mathbf{R}_j = (R_{ml}^{(+j)}) \quad \text{for } j = 1, \dots, N_\mathrm{s},$$

$$\mathbf{T}_j = (T_{ml}^{(+j)}) \quad \text{for } j = 1, \dots, N_\mathrm{s},$$

$$\mathbf{R}_{-j} = (R_{ml}^{(-j)}) \quad \text{for } j = 1, \dots, N_\mathrm{s}-1,$$

$$\mathbf{T}_{-j} = (T_{ml}^{(-j)}) \quad \text{for } j = 1, \dots, N_\mathrm{s}-1 \tag{52}$$

($m = -n_\mathrm{r}, \dots, n_\mathrm{r}$; $l = -n_\mathrm{r}, \dots, n_\mathrm{r}$).

Now we consider an elastic medium partitioned by two imperfectly bonded interfaces as an example (Fig. 3). When an upgoing wave denoted by $\mathbf{A}_1$ is incident on the first interface, $\mathbf{B}_1$ and $\mathbf{A}_3$ can be written in the form

$$\mathbf{B}_1 = \mathbf{R}_{12}\mathbf{A}_1, \tag{53}$$

$$\mathbf{A}_3 = \mathbf{T}_{12}\mathbf{A}_1, \tag{54}$$

where $\mathbf{R}_{12}$ and $\mathbf{T}_{12}$ are the reflection and transmission matrices of the second layer for upgoing incident waves. We obtain the following expressions for $\mathbf{R}_{12}$ and $\mathbf{T}_{12}$:

$$\mathbf{R}_{12} = \mathbf{R}_1 + \mathbf{T}_{-1}\mathbf{R}_2(\mathbf{I} - \mathbf{R}_{-1}\mathbf{R}_2)^{-1}\mathbf{T}_1, \tag{55}$$

$$\mathbf{T}_{12} = \mathbf{T}_2(\mathbf{I} - \mathbf{R}_{-1}\mathbf{R}_2)^{-1}\mathbf{T}_1, \tag{56}$$

where we have used the identity (Kennett 1984)

$$(\mathbf{I} - \mathbf{X})^{-1} = \mathbf{I} + \mathbf{X} + \mathbf{X}^2 + \dots + \mathbf{X}^n(\mathbf{I} - \mathbf{X})^{-1}. \tag{57}$$

The expressions for $\mathbf{A}_2$ and $\mathbf{B}_2$ can be obtained in the same way, as follows:

$$\mathbf{A}_2 = (\mathbf{I} - \mathbf{R}_{-1}\mathbf{R}_2)^{-1}\mathbf{T}_1\mathbf{A}_1, \tag{58}$$

$$\mathbf{B}_2 = \mathbf{R}_2(\mathbf{I} - \mathbf{R}_{-1}\mathbf{R}_2)^{-1}\mathbf{T}_1\mathbf{A}_1. \tag{59}$$

Thus we can calculate the displacement field anywhere in the medium. In addition, we can obtain the expressions for the matrices $\mathbf{R}_{21}$ and $\mathbf{T}_{21}$ for downgoing incident waves in the

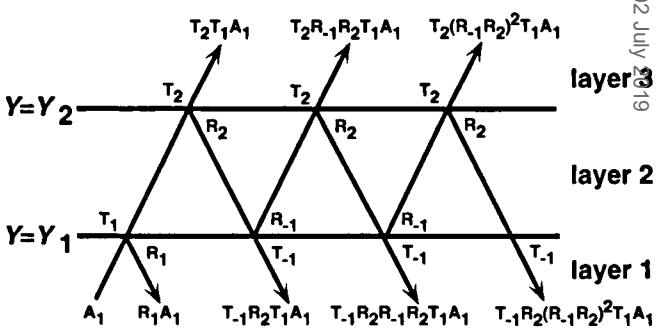

Figure 3. Some rays propagating in a medium partitioned by two imperfectly bonded interfaces.

same way. The expressions for these matrices are

$$\mathbf{R}_{21} = \mathbf{R}_{-2} + \mathbf{T}_2\mathbf{R}_{-1}(\mathbf{I} - \mathbf{R}_2\mathbf{R}_{-1})^{-1}\mathbf{T}_{-2}, \quad (60)$$

$$\mathbf{T}_{21} = \mathbf{T}_{-1}(\mathbf{I} - \mathbf{R}_2\mathbf{R}_{-1})^{-1}\mathbf{T}_{-2}. \quad (61)$$

When we consider a multilayered zone partitioned by many imperfectly bonded interfaces, we can calculate the reflection and transmission matrices of any region and the displacement field in any position by the procedure described above.

4 SCATTERING BY A SINGLE ARRAY OF CRACKS

4.1 Accuracy of the method of solution

In this section, we check the accuracy of the method described in Section 2 by comparison with the solution given by Achenbach & Li (1986) for scattering of *SH* waves by a periodic array of stress-free cracks. These authors derived the solution by expanding the relative displacement at a crack in Chebyshev polynomials and taking advantage of the geometrical periodicity. We assume a periodic array of cracks as illustrated in Fig. 4, where a is half the crack length and d is the spacing between cracks. Achenbach & Li assumed that the reflected waves could be expressed as the following superposition of plane waves:

$$u_R(x, y) = \sum_{m=-\infty}^{\infty} \Phi_m \exp[\mathrm{i}(k\cos\varphi + 2\pi m/d)x + \beta_2(k\cos\varphi + 2\pi m/d)y] \quad \text{for } y < 0. \quad (62)$$

They calculated only the zeroth-order reflection coefficient $|\Phi_0|$. This is defined as the coefficient of the reflected-wave component that has a reflection angle equal to the incidence angle. The zeroth-order reflection coefficient $|\Phi_0|$ is equal to $|1 - (\mathrm{i}/2\pi)C_0|$ in eq. (12) with C_0 as defined by eq. (14). Let us now compare the zeroth-order reflection coefficient obtained by the method of Achenbach & Li with ours for the cases $d = 4.0a$ and $d = 2.5a$ and check the accuracy of our method, which we refer to as the discrete plane-wave expansion method (DPEM). The crack distribution in the DPEM is represented by spatial inhomogeneity in the specific stiffness function as stated above, and it is assumed to be as shown in Fig. 5. The stiffness $k_T(x)$ should be infinitely large for an intact section; we arbitrarily assume $k_T(x) = 100\mu/a$. The assumption

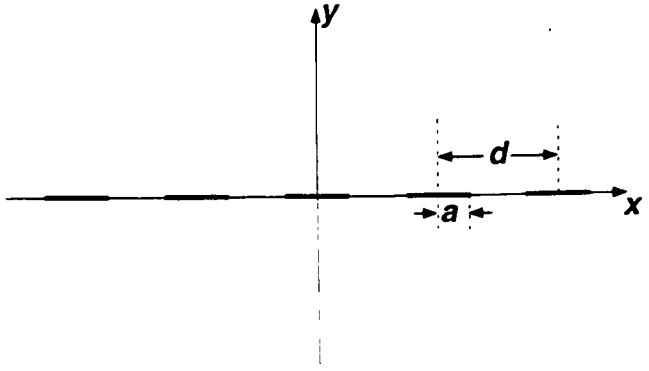

Figure 4. A single periodic array of cracks; a is half the crack length and d is the crack spacing.

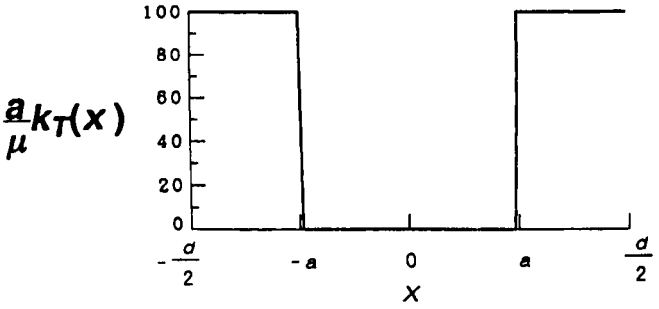

Figure 5. The specific stiffness function for the periodic array of cracks shown in Fig. 4. We assume $k_T(x) = 100\mu/a$ for an intact section.

of much larger values for $k_T(x)$ causes little difference in the calculated results. We need to assume a larger number for N in eq. (9) to approximate a discontinuity in $k_T(x)$ with higher precision. In Fig. 6, we show the solution C_m as defined in eq. (14) at different wavenumbers for the case of $d = 2.5a$ and $\varphi = 90°$, as an example. This figure clearly shows the rapid attenuation of $|C_m|$ with increasing $|m|$ for all assumed values of ka. Our experience with these calculations shows that truncation of the series of values of C_m at $n = 3N/2$ is sufficient (see Fig. 6); there is little difference in the calculated results if more plane-wave components are assumed in the truncated forms of eqs (12) and (13).

Fig. 7 compares the zeroth-order reflection coefficients R_0 obtained by Achenbach & Li (1986) with those obtained from the DPEM in our study, for $\varphi = 90°$ (Fig. 7a) and 45° (Fig. 7b). The reflection coefficient is zero for an incident wave of infinitely long wavelength. This is because the displacement in an *SH* wave is independent of y for $ka \sim 0$, so that no relative displacement occurs at the interface (see eq. 5). The reflection coefficient increases monotonically with increasing ka up to a certain value, and then abrupt changes occur at some wavenumbers. According to Achenbach & Li (1986), such abrupt changes occur at those wavenumbers where a higher-order mode ($m = \pm 1, \pm 2, \ldots$) in eq. (62) changes from an evanescent mode to a homogeneous one; the abrupt changes occur at values of ka which satisfy the following equation:

$$ka = \pm\left(ka\cos\varphi + \frac{2a}{d}m\pi\right), \quad m = 1, 2, \ldots. \quad (63)$$

We find that our results represent the discontinuous slopes successfully; these results confirm that the accuracy of our method of analysis is satisfactory.

As another independent check, we compared the relative displacement calculated by the DPEM with that calculated by a boundary integral equation method (BIEM) employed by Murai *et al.* (1995). While the BIEM faces a difficulty of memory and CPU-time limits in dealing with large numbers of cracks, it is a well-developed method and Murai *et al.* (1995) confirmed the accuracy of their method with some examples. Fig. 8 shows the relative displacement for the case of a single periodic array of cracks, for $d = 2.5a$ and $\varphi = 90°$. The solution shown for the BIEM is the relative displacement for a crack in the centre of an array of 25 cracks. This figure shows excellent agreement between the results for all values of ka used. The relative displacement spreads slightly into the intact section in the DPEM solution. This is due to the finiteness of the specific stiffness function for the intact section, which is

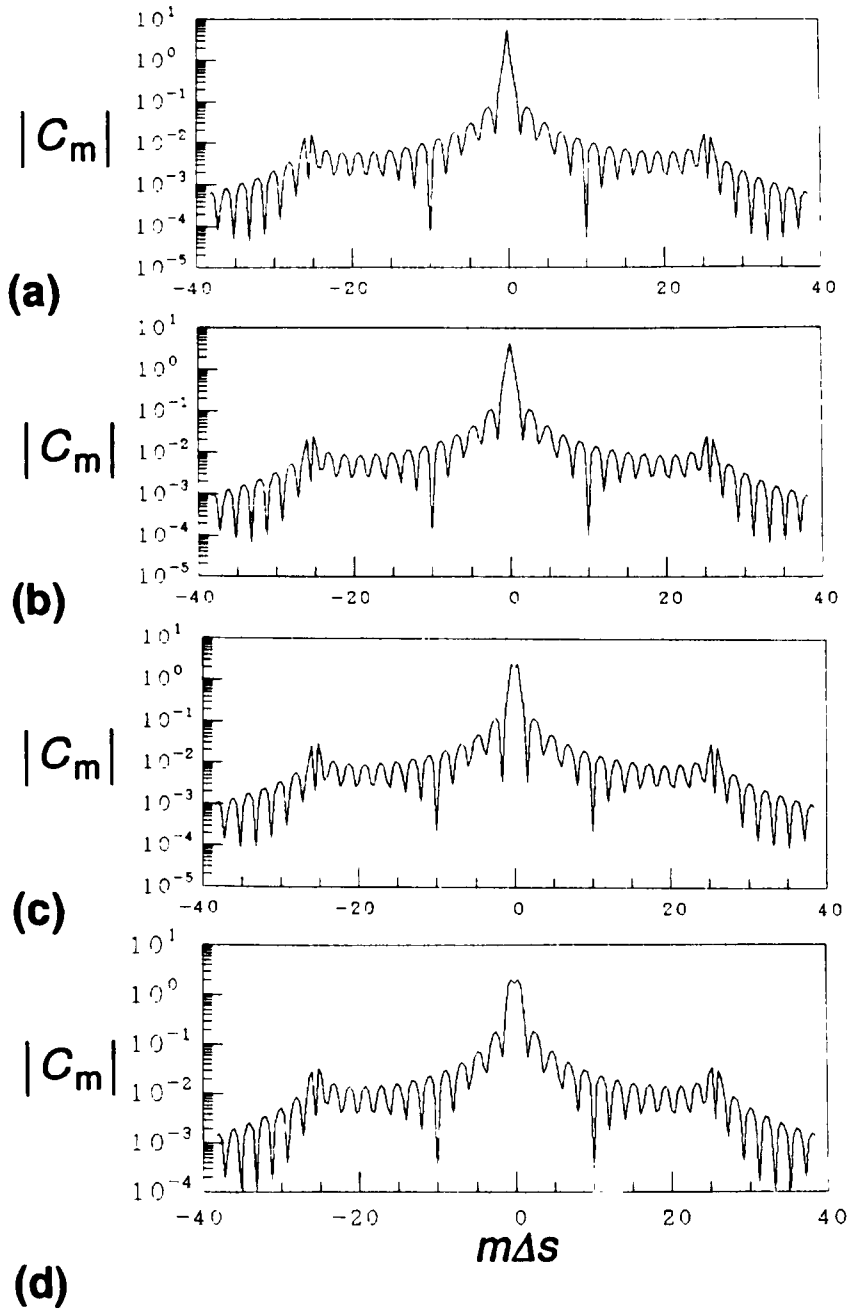

Figure 6. The solution C_m as a function of wavenumber for the case $d = 2.5a$ and $\varphi = 90°$. The values of ka are (a) 0.5, (b) 1.0, (c) 2.0 and (d) 4.0. We have taken $N = 64$ and $n = 96$ in this computation.

inevitable in a numerical treatment. If we assume a larger value of $k_T(x)$ for the intact sections, we can reduce this spreading effect. These small displacements in the intact sections have been shown to cause negligible effect on the scattered waves.

4.2 The effect of viscous friction acting at the crack surfaces

In this section, we now make a short analysis of the effect of viscous friction acting at the crack surfaces. We assume that each crack contains a very thin cavity filled with a Newtonian fluid with viscosity coefficient η. Although the mean thickness ε of the cavity is negligibly small, its value is assumed to affect the strength of the viscous friction acting at the crack surfaces. We employ the specific viscosity function $\eta^*(x) = \eta/\varepsilon = \sigma\mu/\beta$ for the cracked sections in the calculation. The effect of viscous friction is illustrated in Fig. 9 for normal incidence on the crack surfaces ($\varphi = 90°$); $d = 4.0a$ is assumed here. When $\sigma = 0.0$, the crack surfaces are stress-free and the reflection coefficient is the same as that in Fig. 7(a). It is observed, however, that the zeroth-order reflection coefficient is smaller for $\sigma = 0.5$ than for $\sigma = 0.0$. This is because the viscous friction tends to suppress slip along the cracks, so that the amplitude of the reflected waves is smaller.

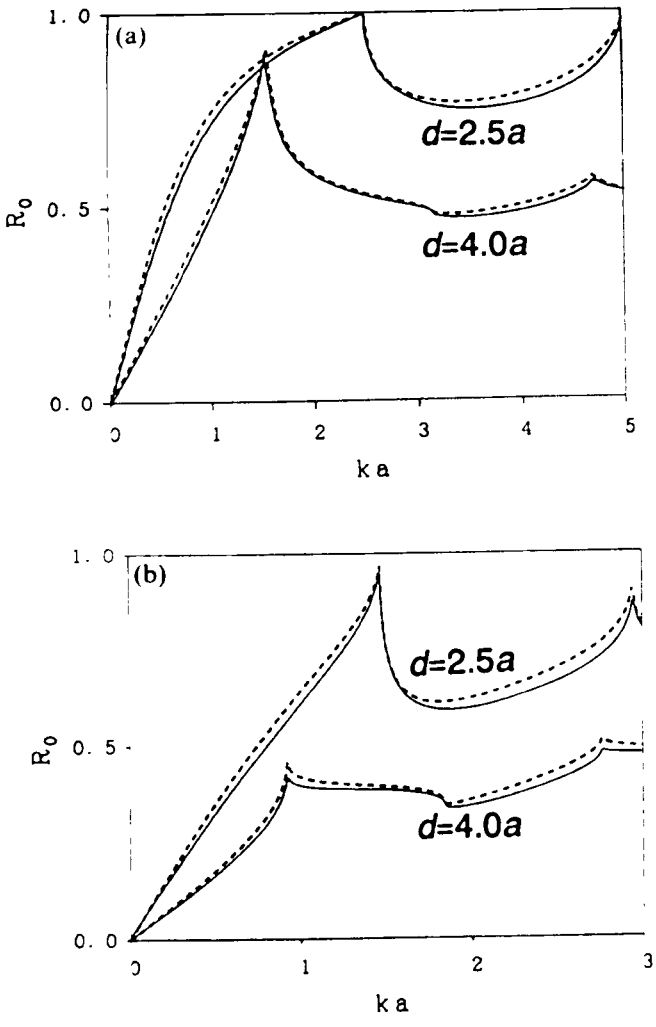

Figure 7. The zeroth-order reflection coefficients R_0 of a single periodic array of cracks. The incidence angles φ are (a) 90 and (b) 45 . The solid curves are the solution given by Achenbach & Li (1986) (reproduced by kind permission of Elsevier Science, Amsterdam), while the broken curves are the solutions obtained from the DPEM, with $N = 64$ and $n = 96$

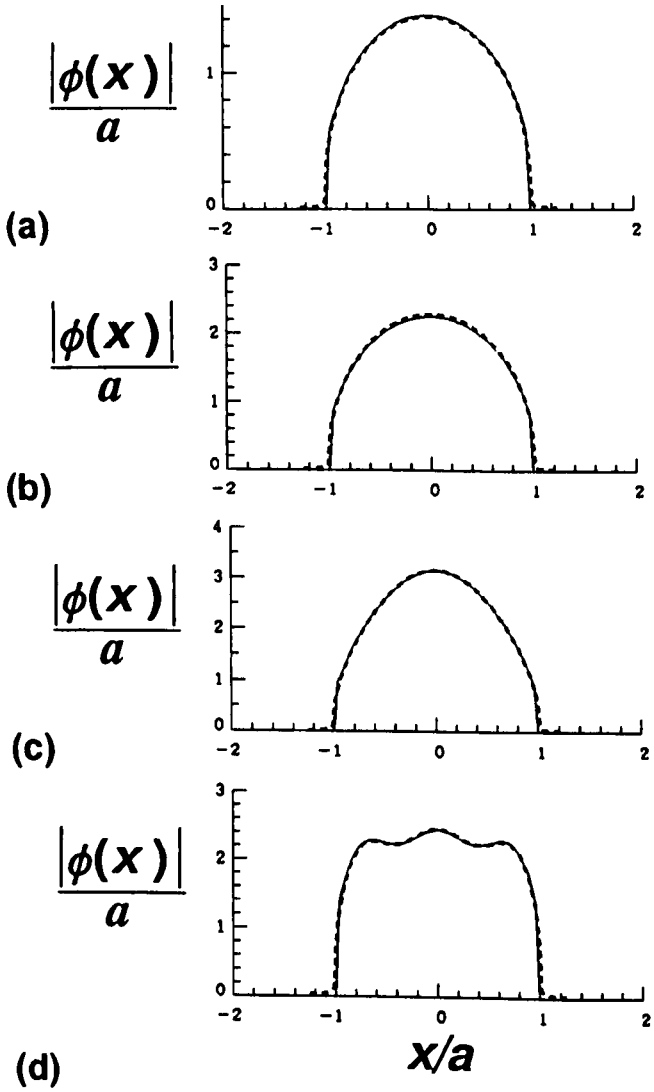

Figure 8. Comparison of the relative displacements $\phi(x)$ obtained by the method of Murai *et al.* (1995) and by the DPEM for the case of a single periodic array of cracks ($d = 2.5a$). Normal incidence to the crack array ($\varphi = 90°$) is assumed. The values of ka are (a) 0.5, (b) 1.0, (c) 2.0 and (d) 4.0. The solid curves denote the solution obtained by the method of Murai *et al.*, while the broken curves denote the solution obtained by the DPEM. For the method of Murai *et al.*, each crack surface was discretized into 50 segments and the solution shown here is the relative displacement of a crack in the centre of an array of 25 cracks.

5 SCATTERING BY A DOUBLE ARRAY OF CRACKS

5.1 Accuracy of the method of solution

In this section, we check the accuracy of our treatment for zonally distributed cracks. As one of the simplest examples we assume a double array of cracks as shown in Fig. 10(a). The crack spacings are $4.0a$ in the X direction and $0.1a$ in the Y direction. No viscous friction is assumed at the crack surfaces. Because there is no available reference for comparison, we compare the relative displacements given by the DPEM with those given by the method of Murai *et al.* (1995), as in Section 4.1. The same specific stiffness function is assumed as in Fig. 5. The relative displacement for the crack distribution in Fig. 10(a) is shown in Fig. 11. The wave propagator method was coupled to the DPEM for the calculation of the scattered waves. This figure shows excellent agreement between the results of our method and that of Murai *et al.* (1995) for all values assumed for ka, in spite of the narrow spacing of the crack arrays in the Y direction. In addition, we find that the reflection and transmission operator method coupled to the DPEM also gives satisfactory results for the crack distribution in Fig. 10(a). Thus the accuracy of the method proposed in this paper is shown to be quite satisfactory.

5.2 The zeroth-order reflection coefficients

As stated before, the zeroth-order reflection coefficient is defined as the coefficient for a reflected-wave component that has its reflection angle equal to the incidence angle, so that the zeroth-order reflection coefficient R_0 is given by $|B_{10}|$ in eq. (23) or eq. (45) in the case of the model of a double crack array.

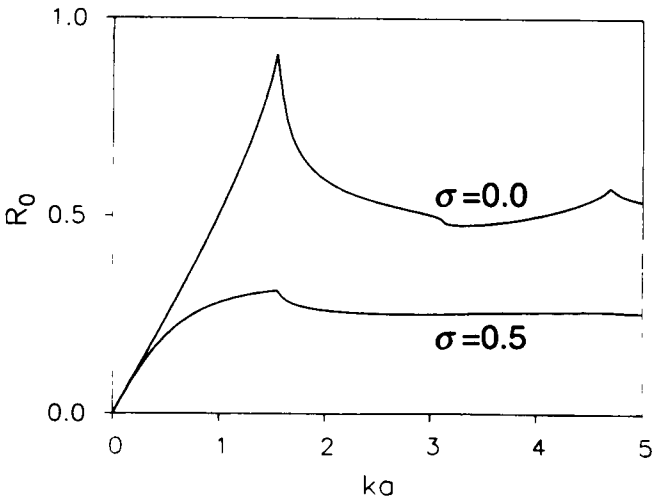

Figure 9. The zeroth-order reflection coefficients R_0 of a single periodic array of cracks ($d = 4.0a$). Normal incidence to the crack array ($\varphi = 90°$) is assumed. The crack surfaces are either stress-free ($\sigma = 0.0$) or subject to viscous friction ($\sigma = 0.5$). We have taken $N = 64$ and $n = 96$ in this computation.

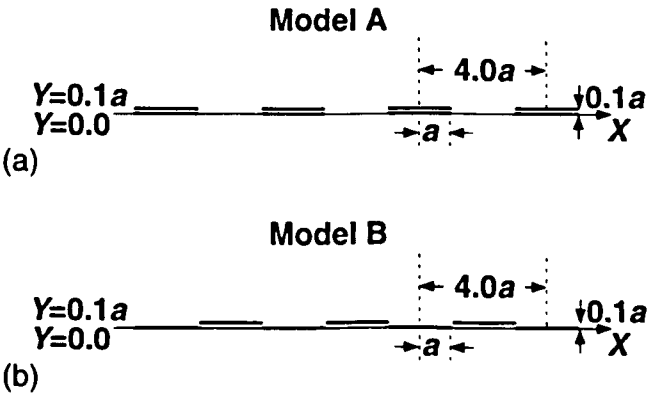

Figure 10. Two double periodic arrays of cracks; a is half the crack length. The crack spacings are $4.0a$ in the X direction and $0.1a$ in the Y direction. The two arrays of cracks (at $Y = 0$ and $Y = 0.1a$) overlap in (a) (Model A), while they do not in (b) (Model B).

We assume two models for the distribution of cracks as shown in Fig. 10. The crack spacings are the same in the two models. The arrays of cracks at $Y = 0$ and $Y = 0.1a$ overlap each other in Fig. 10(a), while they do not in Fig. 10(b); the models shown in Figs 10(a) and (b) are referred to here as models A and B, respectively. The specific stiffness function illustrated in Fig. 5 is assumed, and no viscous friction is assumed at the crack surfaces. The zeroth-order reflection coefficients for these models are shown in Fig. 12 for normal incidence of plane waves. We used the wave propagator method in this computation. The overall wavenumber dependence of the reflection coefficient for model A seems to be quite similar to that for the case of $d = 4.0a$ shown in Fig. 7(a). This is because an overlapping, double array of cracks tends to behave like a single array of cracks for incident waves whose wavelengths are much longer than the crack spacing in the Y direction. The sharp change in reflection coefficient observed at around $ka = 1.57$ in the plots for $d = 4.0a$ in Fig. 7(a) and for model A in Fig. 12 is lost in the reflection coefficient for model B. The wavenumber dependence for model B is similar to that for the case of an imperfectly bonded interface with a spatially homogeneous strength (Schoenberg 1980). This is because a double array of cracks of the kind shown in Fig. 10(b) tends to behave like a single fracture for incident waves of long wavelength.

6 CONCLUSIONS

We have developed a new, simple method to treat multiple scattering of elastic waves due to zonally distributed parallel cracks. In our formulation, arbitrarily distributed parallel cracks are represented by imperfectly bonded parallel interfaces with spatially inhomogeneous strengths. A section with zero strength denotes a stress-free crack, while a section with a significantly high elastic stiffness approximates an intact section. In this formulation, an array of cracks is represented by a single interface and the interactions between all cracks are considered implicitly. This approach can circumvent the mixed boundary condition that has to be solved in the traditional approach to the crack scattering problem.

The scattered waves are expanded into discrete reflected and transmitted plane-wave components in our method. The displacement field in a zone partitioned by many imperfectly bonded interfaces, which is a model for a cracked zone, can be calculated by the wave propagator method or by the reflection and transmission operator method once the reflection and transmission coefficients of each interface have been obtained. It has been shown that the accuracy of this method is quite satisfactory for *SH*-wave scattering due to single and double periodic arrays of cracks.

The wave propagator method and the reflection and transmission operator method each have advantages and disadvantages. The wave propagator method calculates the upgoing and downgoing wave components together. Therefore it takes less time for the calculation, but it is impossible to calculate for high wavenumbers or in the case of a thick layer. On the other hand, the reflection and transmission operator method can be used in any situation because it treats the upgoing and downgoing waves separately. However, a long computational time is generally required (Kennett 1983; Koketsu & Takenaka 1989).

The zeroth-order reflection coefficient, defined as the coefficient for a reflected-wave component having a reflection angle equal to the incidence angle, has been calculated for some crack arrays, and its dependence on the crack configuration and crack face coupling has been investigated. When the crack surfaces are subject to viscous friction, the reflection coefficient is smaller than it is in the case of stress-free crack surfaces. This is because the viscous friction tends to suppress slip along the cracks, so that the amplitude of the reflected waves is smaller. In the case of a closely spaced double array of cracks, the reflection coefficient has a wavenumber dependence similar to that for a single array of cracks, when one array is hidden from an incident plane wave behind the other array. On the other hand, the wavenumber dependence is similar to that for an imperfectly bonded interface with spatially homogeneous strength when the two arrays of cracks do not overlap. This is because an overlapping double array of cracks tends to behave like a single array of cracks for incident waves of long wavelength, while a non-overlapping double array of cracks tends to behave like a single fracture.

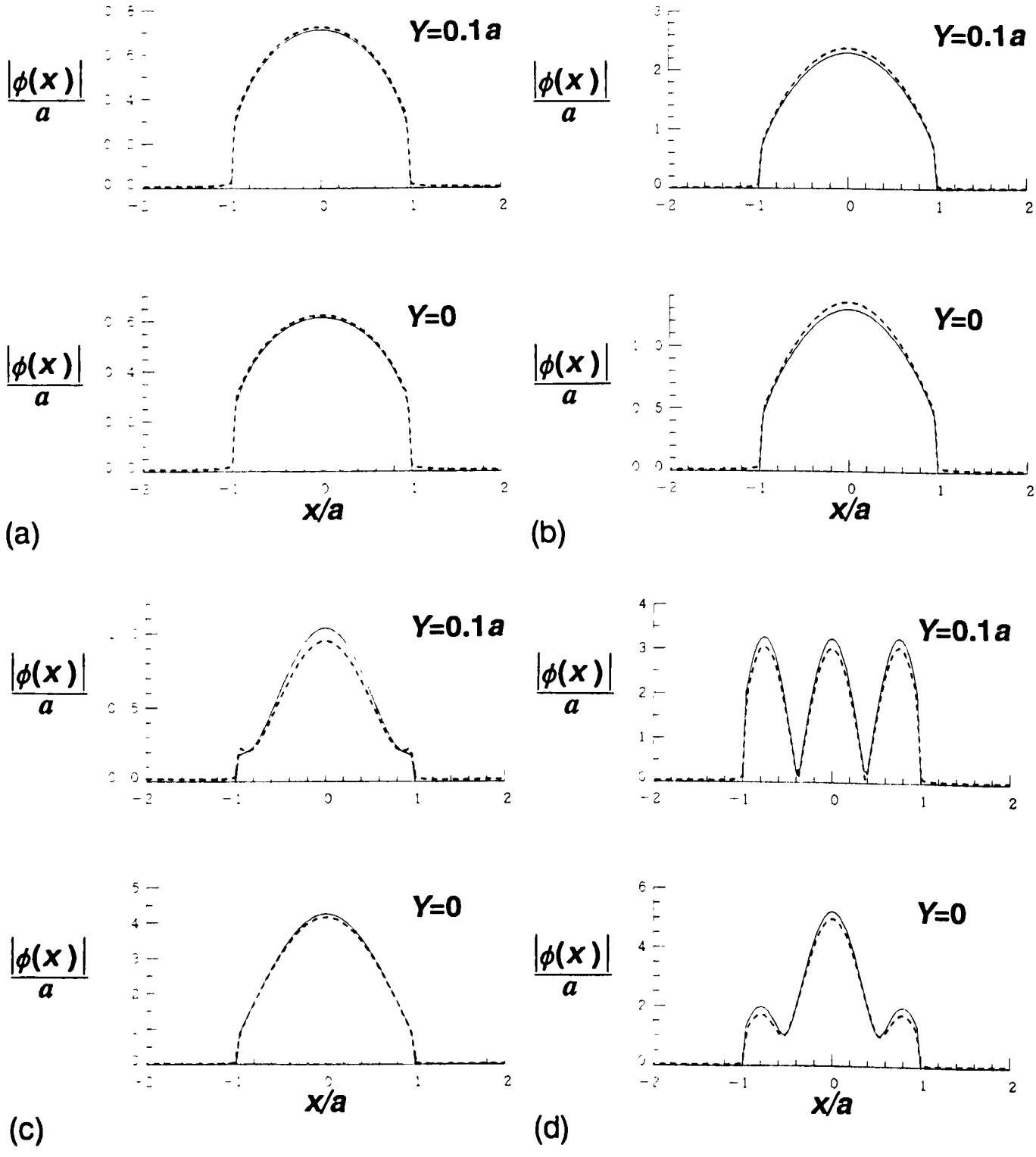

Figure 11. Comparison of the relative displacements $\phi(x)$ obtained by the method of Murai *et al.* (1995) (solid curve) and by the wave propagator method coupled to the DPEM (broken curve) for the double periodic array of cracks shown in Fig. 10(a). Normal incidence to the crack array ($\varphi = 90°$) is assumed. The values of ka are (a) 0.5, (b) 1.0, (c) 2.0 and (d) 4.0. In each part of the figure, the top and bottom show the relative displacements at the cracks at $Y = 0.1a$ and $Y = 0$, respectively. For the method of Murai *et al.*, each crack surface was discretized into 50 segments and the solution shown here is the relative displacement of a crack in the centre of an array of 11 cracks on each of the planes $Y = 0.1a$ and $Y = 0$. We have taken $N = 64$ and $n = 96$ in the DPFM, and $n_e = 96$ in computing the evanescent waves; n_p and n_q were determined so that $\exp[-0.1a\beta_2(k\cos\varphi + 2\pi m\Delta s)] \geq 0.1$ and $-n_q \leq m \leq n_p$ were satisfied for each wavenumber in computing the wave propagator. The factor $\exp[-\beta_2(k\cos\varphi + 2\pi m\Delta s)(Y_2 - Y_1)]$ occurs in the representation of the reflection and transmission coefficients in Appendix A.

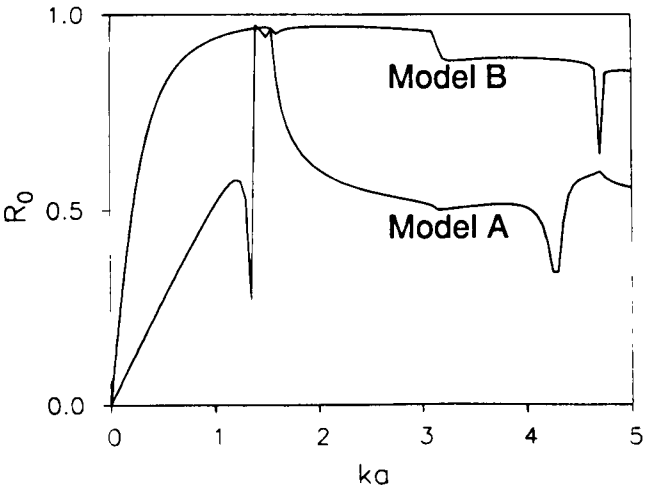

Figure 12. The zeroth-order reflection coefficients R_0 of the double periodic arrays of cracks shown in Fig. 10. Normal incidence to the crack array ($\varphi = 90^\circ$) is assumed. The values of the parameters in this computation were the same as in Fig. 11.

The method proposed in this paper has the advantages that multiple elastic wave scattering due to large numbers of densely distributed cracks is easily treated and that arbitrary coupling of crack surfaces is easily introduced. The introduction of a low-velocity zone is also easy in our method because we have only to consider the reflection and transmission of plane waves (Murai 1994). Therefore, our method of analysis can be a useful mathematical tool to analyse wave propagation in a zone permeated by large numbers of densely distributed cracks. In future papers, (Y. Murai, in preparation) we will model a fault zone as a cracked zone and calculate its response to incident elastic waves by the method proposed in this paper. Moreover, we will try to estimate crack lengths in the fault zone of the 1992 Landers, California, earthquake from the trapped waves observed by Li *et al.* (1994).

ACKNOWLEDGMENTS

We have used the computer systems of the Earthquake Information Centre of the Earthquake Research Institute, University of Tokyo for this study. The authors wish to thank the anonymous reviewer for helpful comments.

REFERENCES

Achenbach, J.D. & Li, Z.L., 1986. Reflection and transmission of scalar waves by a periodic array of screens, *Wave Motion*, **8**, 225–234.

Foldy, L.L., 1945. The multiple scattering of waves. I. General theory of isotropic scattering by randomly distributed scatterers, *Phys. Rev.*, **67**, 107–119.

Hudson, J.A., Liu, E. & Crampin, S., 1996. Transmission properties of a plane fault, *Geophys. J. Int.*, **125**, 559–566.

Kawahara, J. & Yamashita, T., 1992. Scattering of elastic waves by a fracture zone containing randomly distributed cracks, *Pageoph*, **139**, 121–144.

Kennett, B.L.N., 1983. *Seismic Wave Propagation in Stratified Media*, Cambridge University Press, Cambridge.

Kennett, B.L.N., 1984. Reflection operator methods for elastic waves II composite regions and source problems, *Wave Motion*, **6**, 419–429.

Kikuchi, M., 1981a. Dispersion and attenuation of elastic waves due to multiple scattering from inclusions, *Phys. Earth planet. Inter.*, **25**, 159–162.

Kikuchi, M., 1981b. Dispersion and attenuation of elastic waves due to multiple scattering from cracks, *Phys. Earth planet. Inter.*, **27**, 100–105.

Koketsu, K. & Takenaka, H., 1989. Review: theories on wave propagation in the near field of seismic sources, *Zisin*, Ser. 2, **42**, 391–403 (in Japanese).

Leary, P.C., Li, Y.-G. & Aki, K., 1987. Observation and modelling of fault-zone fracture seismic anisotropy—I. *P*, *SV* and *SH* travel times, *Geophys. J. R. astr. Soc.*, **91**, 461–484.

Li, Y.-G., Leary, P.C. & Aki, K., 1987. Observation and modelling of fault-zone fracture seismic anisotropy—II. *P*-wave polarization anomalies, *Geophys. J. R. astr. Soc.*, **91**, 485–492.

Li, Y.-G., Aki, K., Adams, D. & Hasemi, A., 1994. Seismic guided waves trapped in the fault zone of the Landers, California, earthquake of 1992, *J. geophys. Res.*, **99**, 11 705–11 722.

Malin, P.E., Waller, J.A., Borcherdt, R.D., Cranswick, E., Jensen, E.G. & Van Schaack, J., 1988. Vertical seismic profiling of Oroville microearthquakes: velocity spectra and particle motion as a function of depth, *Bull. seism. Soc. Am.*, **78**, 401–420.

Murai, Y., 1994. Theoretical study on response of a fault zone to elastic waves, *DSc thesis*, University of Tokyo.

Murai, Y., Kawahara, J. & Yamashita, T., 1995. Multiple scattering of *SH* waves in 2-D elastic media with distributed cracks, *Geophys. J. Int.*, **22**, 925–937.

Nagy, P.B., 1992. Ultrasonic classification of imperfect surfaces, *J. nondestr. Eval.*, **11**, 127–139.

Ohnaka, M., Kuwahara, Y. & Yamamoto, K., 1987. Constitutive relations between dynamic physical parameters near a tip of the propagating slip zone during stick-slip shear failure, *Tectonophysics*, **144**, 109–125.

Pyrak-Nolte, L.J. & Cook, N.G.W., 1987. Elastic interface waves along a fracture, *Geophys. Res. Lett.*, **14**, 1107–1110.

Schoenberg, M., 1980. Elastic wave behavior across linear slip interfaces, *J. acoust. Soc. Am.*, **68**, 1516–1521.

Schoenberg, M. & Douma, J., 1988. Elastic wave propagation in media with parallel fractures and aligned cracks, *Geophys. Prospect.*, **36**, 571–590.

Takeshita, T. & Karato, S., 1989. Anisotropy in the Earth formed by plastic flow in rocks, *Zisin*, Ser. 2, **42**, 255–269 (in Japanese).

Yamashita, T., 1990. Attenuation and dispersion of *SH* waves due to scattering by randomly distributed cracks, *Pageoph*, **132**, 545–568.

Yoshioka, N. & Kikuchi, M., 1993. Visco-elastic response of joints to transmission waves, *Geophys. Res. Lett.*, **20**, 1143–1146.

APPENDIX A: REPRESENTATION OF THE REFLECTION AND TRANSMISSION COEFFICIENTS

We define here the notation for the reflection and transmission coefficients at each interface. See eq. (27) for the definition of $e_m^{(+j)}$. An upgoing plane-wave component $e_l^{(-j)}$ is assumed to be incident on the jth interface. The reflected waves are expanded into the downgoing plane-wave components $R_{ml}^{(+j)} e_m^{[+(j-1)]}$ (for $j = 2, \ldots, N_s$) or $R_{ml}^{(+1)} e_m^{(+1)}$ (for $j = 1$) and the transmitted waves are expanded into the upgoing plane-wave components $T_{ml}^{(+j)} e_m^{[-(j+1)]}$ (for $j = 1, \ldots, N_s - 1$) or $T_{ml}^{(+N_s)} e_m^{(-N_s)}$ (for $j = N_s$), where $R_{ml}^{(+j)}$ and $T_{ml}^{(+j)}$ are the reflection and transmission coefficients, respectively, at the jth interface. The reflection and transmission coefficients for a downgoing incident plane-wave component are denoted by $R_{ml}^{(-j)}$ and $T_{ml}^{(-j)}$ in a similar way. These reflection and transmission coefficients are derived from the solution C_m defined in eq. (14). We rewrite the C_m of the jth interface for an incident plane-wave component $e_l^{(-j)}$ as $C_{ml}^{(j)}$. Then the reflection and

transmission coefficients are obtained explicitly as follows. When $j = 1$,

$$R_{mm}^{(+1)} = 1 - \frac{1}{2\pi} C_{mm}^{(1)}, \tag{A1}$$

$$R_{ml}^{(+1)} = -\frac{1}{2\pi} C_{ml}^{(1)} \quad \text{for } m \neq l, \tag{A2}$$

$$T_{ml}^{(+1)} = \frac{1}{2\pi} C_{ml}^{(1)} \exp[\mathrm{i}(k\cos\varphi + 2\pi m\Delta s)(X_2 - X_1) - \beta_2(k\cos\varphi + 2\pi m\Delta s)(Y_2 - Y_1)], \tag{A3}$$

$$R_{mm}^{(-1)} = \left(1 - \frac{1}{2\pi} C_{mm}^{(1)}\right) \exp[\mathrm{i}(k\cos\varphi + 2\pi m\Delta s)(X_2 - X_1) - \beta_2(k\cos\varphi + 2\pi m\Delta s)(Y_2 - Y_1)], \tag{A4}$$

$$R_{ml}^{(-1)} = -\frac{\mathrm{i}}{2\pi} C_{ml}^{(1)} \exp[\mathrm{i}(k\cos\varphi + 2\pi m\Delta s)(X_2 - X_1) - \beta_2(k\cos\varphi + 2\pi m\Delta s)(Y_2 - Y_1)] \quad \text{for } m \neq l, \tag{A5}$$

$$T_{ml}^{(-1)} = \frac{1}{2\pi} C_{ml}^{(1)}. \tag{A6}$$

When $j = 2, \ldots, N_s - 1$,

$$R_{mm}^{(+j)} = \left(1 - \frac{1}{2\pi} C_{mm}^{(j)}\right) \exp[-\mathrm{i}(k\cos\varphi + 2\pi m\Delta s)(X_j - X_{j-1}) - \beta_2(k\cos\varphi + 2\pi m\Delta s)(Y_j - Y_{j-1})], \tag{A7}$$

$$R_{ml}^{(+j)} = -\frac{\mathrm{i}}{2\pi} C_{ml}^{(j)} \exp[-\mathrm{i}(k\cos\varphi + 2\pi m\Delta s)(X_j - X_{j-1}) - \beta_2(k\cos\varphi + 2\pi m\Delta s)(Y_j - Y_{j-1})] \quad \text{for } m \neq l, \tag{A8}$$

$$T_{ml}^{(+j)} = \frac{\mathrm{i}}{2\pi} C_{ml}^{(j)} \exp[\mathrm{i}(k\cos\varphi + 2\pi m\Delta s)(X_{j+1} - X_j) - \beta_2(k\cos\varphi + 2\pi m\Delta s)(Y_{j+1} - Y_j)], \tag{A9}$$

$$R_{mm}^{(-j)} = \left(1 - \frac{\mathrm{i}}{2\pi} C_{mm}^{(j)}\right) \exp[\mathrm{i}(k\cos\varphi + 2\pi m\Delta s)(X_{j+1} - X_j) - \beta_2(k\cos\varphi + 2\pi m\Delta s)(Y_{j+1} - Y_j)], \tag{A10}$$

$$R_{ml}^{(-j)} = -\frac{\mathrm{i}}{2\pi} C_{ml}^{(j)} \exp[\mathrm{i}(k\cos\varphi + 2\pi m\Delta s)(X_{j+1} - X_j) - \beta_2(k\cos\varphi + 2\pi m\Delta s)(Y_{j+1} - Y_j)] \quad \text{for } m \neq l, \tag{A11}$$

$$T_{ml}^{(-j)} = \frac{\mathrm{i}}{2\pi} C_{ml}^{(j)} \exp[-\mathrm{i}(k\cos\varphi + 2\pi m\Delta s)(X_j - X_{j-1}) - \beta_2(k\cos\varphi + 2\pi m\Delta s)(Y_j - Y_{j-1})]. \tag{A12}$$

When $j = N_s$,

$$R_{mm}^{(+N_s)} = \left(1 - \frac{\mathrm{i}}{2\pi} C_{mm}^{(N_s)}\right) \exp[-\mathrm{i}(k\cos\varphi + 2\pi m\Delta s) \times (X_{N_s} - X_{N_s-1}) - \beta_2(k\cos\varphi + 2\pi m\Delta s)(Y_{N_s} - Y_{N_s-1})], \tag{A13}$$

$$R_{ml}^{(+N_s)} = -\frac{\mathrm{i}}{2\pi} C_{ml}^{(N_s)} \exp[-\mathrm{i}(k\cos\varphi + 2\pi m\Delta s)(X_{N_s} - X_{N_s-1}) - \beta_2(k\cos\varphi + 2\pi m\Delta s)(Y_{N_s} - Y_{N_s-1})] \quad \text{for } m \neq l, \tag{A14}$$

$$T_{ml}^{(+N_s)} = \frac{\mathrm{i}}{2\pi} C_{ml}^{(N_s)}. \tag{A15}$$